An Artificial Compound Eye Tracking Pan-Tilt Motion

Gwo-Long Lin and Chi-Cheng Cheng

***Abstract*—The compound eyes of an insect can focus on prey accurately and quickly. From biological perspective, compound eyes are excellent at detecting motion. Based on the computer vision aspect, limited studies regarding this issue exist. Studies have verified that a trinocular visual system incorporating a third CCD camera into a conventional binocular is very helpful in resolving translational motion. Extended from this concept, this study presents a novel spherical compound-like eye of a superposition type for pan-tilt rotational motion. We conclude that as the number of ommatidium an insect has increased, capability for detecting prey increases, even for ambiguous patterns in each ommatidium. In this study, the compound eyes of insects are investigated using computer vision principles.**

***Keywords*—Biological imaging, Superposition-type spherical compound-like eye, Pan-tilt motion detection.**

I. Introduction

The configuration of insect compound eyes has always attracted the attention of researchers. Biology-based visual studies have recently flourished along with a boom in microlens technology. Development of image acquisition systems based on the compound eye framework has progressed more rapidly than ever before. The fabrication of micro-compound eyes has been described in literature with an orientation toward commercial applications. Well-known commercial applications include the Thin Observation Module by Bound Optics (TOMBO) compound eye developed by Tanita *et al*. [1], and the hand-held plenoptic camera developed by Ng *et al.* [2]. The TOMBO compound eye is a multiple-imaging system with a post-digital processing unit that has a compact hardware configuration with processing flexibility. The hand-held plenoptic camera is similar to the plenoptic camera developed by Adelson and Wang [3], but with two fewer lenses, significantly shortening the optical path and resulting in a portable camera. Furthermore, some related image-acquisition systems contain one photoreceptor per view direction [4, 5], a miniaturized imaging system [6], an electronic compound eye [7], curved gradient index lenses [8], an artificial ommatidia [9], and a silicon-based digital retina [10]. All of these are image-acquisition systems that have the framework of a compound eye.

One of the most fundamental features of biological compound eyes is their high sensitivity to moving images. The ability of insects to detect variations in motion vastly surpasses that of human beings and accounts for their skill in locating and capturing prey with unerring speed and accuracy. Although the precise mechanisms responsible for the sensitivity of biological compound eyes have not been conclusively determined, some biologists believe that this ability is because of the flicker effect [11]; that is, as an object moves across a visual field, ommatidia are progressively turned on and off during which bees measure distance based on image motion received by their eyes as they fly [11–16]. Because of the resulting “flicker effect”, insects respond far better to moving than stationary objects. Honeybees, for instance, visit moving flowers more than they do still flowers. Thus, many studies have exerted considerable effort in constructing images viewed from a compound eye and reconstructing an environmental image from those image patterns. Most researches are limited to static images. However, this study focuses on the dynamic vision of a compound eye. To achieve motion recovery for visual servo, ego-motion estimation must be investigated first. Neumann *et al.* [8] applied plenoptic video geometry to construct motion equations, and optimized an error function to acquire motion parameters. Tisse [10] utilized off-the-shelf micro-optical elements to characterize self-motion estimation. Nevertheless, neither study discussed this detection ability for the dynamic vision of the compound eye, nor investigated the noise interference problem. Lin and Cheng [17] recently presented a pan-tilt motion algorithm for a single-row superposition-type spherical compound-like eye (SSCE) for recovery of rotational motion utilizing pinhole perspective projection rather than a complex mathematical interpretation. They indicated that the single-row SSCE generates image information, and markedly improves efficiency and accuracy when estimating motion parameters. Based on this concept, recovery of rotational motion with an SSCE will be examined to generate a complete SSCE framework, rather than limiting this investigation to a single-row SSCE.

This work was funded by National Science Council, Republic of China under contract NSC 93-2212-E-110-014.

Gwo-Long Lin is an assistant professor at the Department of Digital Game Design, Kao Fong College, Chang-Jhih, Pingtung 90841, Taiwan, Republic of China (corresponding phone: +886-8-762-6365#1181; fax: +886-8-800-0329; e-mail: d8932808@student.nsysu.edu.tw).

Chi-Cheng Cheng is a professor at the Department of Mechanical and Electro-Mechanical Engineering of National Sun Yat-Sen University, Kaohsiung 80424, Taiwan, Republic of China (e-mail: chengcc@mail.nsysu.edu.tw).

II. THE COMPOUND-LIKE EYE IN COMPUTER VISION

The mosaic theory of insect vision was proposed by Muller as far back as 1826 and is still generally accepted to this day. According to this theory, there are two compound eye types: apposition and superposition [18]. As the construction of these two eye types are clearly different, the apposition eye acquires images from the ommatidium, and each ommatidium is exploited to make up a complete ambiguous image. The superposition eye can acquire a whole image by adjusting its ommatidia. Each ommatidium can itself capture an ambiguous image, and each image will differ based on different positions. Strictly speaking, superposition here is neural superposition [19, 20]. These two eye types are based on ecology, and can assist in determining how to produce very clear images from compound eyes. However, based on computer vision (CV), which configuration should be adopted? The compound-like eye in CV first proposed by Aloimonos [20] can be classified into two types: a planar compound-like eye; and, a spherical compound-like eye. Fig. 1 depicts the spherical compound-like eye studied in this work.

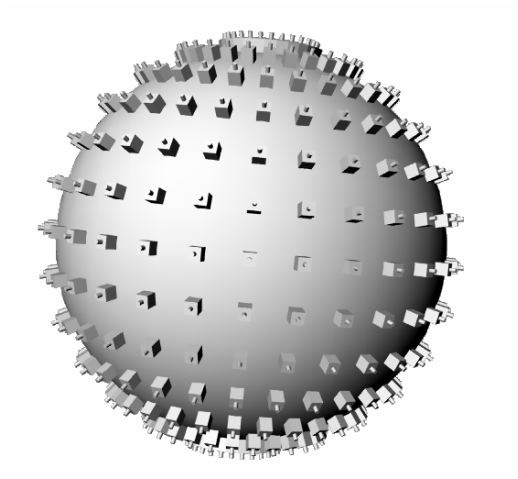

Fig. 1 Compound-like eye of spherical type

The principal research task is to generate the configuration of spherical compound-like eye in CV. First, the configuration of a spherical compound-like eye must be defined. Suppose each ommatidium can look at an object. Based on this scenario, a number of CCD cameras treated as ommatidium are arranged on the sphere surface. The horizontal distance between adjacent ommatidia is fixed. To distinguish the apposition type compound-like eye, this specific arrangement has to be clearly defined as the superposition type. Each ommatidium will have a different and ambiguous view of an object in a noisy environment, not just a small view of an object. Besides, each ommatidium generates its image depending on its different location. The images generated by the SSCE will be vague and undistinguishable, and similar to blurred patterns viewed by insect ommatidia.

III. PAN-TILT EGO-ROTATIONAL MOTION FOR ONE CCD

For analytical purposes, a spherical compound-like eye can be modeled as a pan-tilt compound-like eye system. Assume total rotational angles for both pan and tilt are less than 180°. Based on this specific configuration, normal 3D rotational motion for one CCD can be transformed into 2D rotational motion. After acquiring the pan-tilt ego-rotational motion for one CCD camera, the superposition image of spherical compound-like eyes is discussed in the following section.

To simulate compound-like eyes for an ommatidium looking at an environment, assume an object is moving relative to the CCD platform, and the origin of the CCD platform is located at the optical center of the CCD camera and rotational center of the platform. When a single rigid object is moving, two features must be considered.

1) Using normal 3D rotational motion, pan-tilt rotational motion and image transformation can be established.
2) Based on the image observed by the CCD, the ego-rotational angle of the CCD camera can be resolved.

A. Pan-Tilt Rotation and Image Transformation

Given a world coordinate system, a rotation R applied to a 3D point $P=(X,Y,Z)^T$, which is accomplished through a displacement, $P \to P'$. A normal 3D rotation about an arbitrary axis through the origin of the coordinate system can be described by successive rotations ψ, θ, and ϕ about its Z, Y, and X axes, respectively. Then, transformation M for the arbitrary rigid motion in 3D space is given by M: $P' = RP = R(\psi)R(\theta)R(\phi)P$. Notably, the rotational operations do not commute.

For the composition of an SSCE, each CCD (ommatidium) will match with the cadence of pan-tilt motion and be placed on the sphere surface similar to Fig. 1. This formation approach can generate a compound-like eye pattern. Therefore, rotational motion of the SSCE is basically a simplification of a pure 3D rotational motion; thus, the rotation of the Z axis is set at 0, and only the motion behaviors in the X and Y axes are considered.

First, a 3D point P is moved to a new location by rotating the platform about the X axis by angle ϕ and about the Y axis by angle θ, given as $P \to P'$. Under perspective imaging, point P in 3D space is projected onto a location in the image plane $p=(x,y)^T$. Following the order of pan-tilt rotational motion $R(\theta)R(\phi)$, the rotational motion transformation of the 3D point can be viewed as moving an image point $p=(x,y)$ to a corresponding image point $p'=(x',y')$ based on a 2D image rotational mapping:

3D space point: $R(\theta)R(\phi)\colon P(X,Y,Z) \to P'(X',Y',Z')$
2D image point: $r(\theta)r(\phi)\colon p=(x,y) \to p'=(x',y')$

Therefore, the image point p of P moves to p', and is described by

$$\begin{bmatrix} x' \\ y' \end{bmatrix} = f \begin{bmatrix} x\cos\theta + y\sin\theta\sin\phi + f\sin\theta\cos\phi \\ y\cos\phi - f\sin\phi \end{bmatrix} / \left(-x\sin\theta + y\cos\theta\sin\phi + f\cos\theta\cos\phi\right)$$

where f is the CCD focal length. Notably, this image transformation does not require any information about the scene when the CCD rotates around its lens center.

B. Ego-Rotational Motion of Pan and Tilt

Two image locations, $p_0(x_0, y_0)$ and $p_1(x_1, y_1)$, are projections of a 3D point P at different times, t_0 and t_1. When the image point p_0 moves onto p_1 —assuming no translation occurs—the rotational angles ϕ and θ must be determined.

Image transformation is a forward procedure for image rotational mapping. Computing the amount of rotations from a pair of observations is obviously an inverse problem. To resolve this problem, an intermediate point $p_c(x_c, y_c)$ (Fig. 2) is assumed.

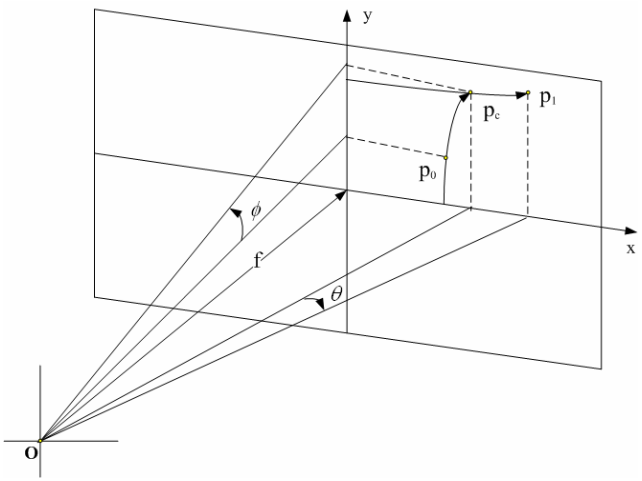

Fig. 2 The rotational path diagram of pan-tilt

As the horizontal rotation and vertical rotation are applied to the CCD separately, Prazdny [21] proved that points in an image move along a hyperbolic path. Similar to the approach developed by Burger and Bhanu [22], the first step is $r(\phi)$, rotation around the X axis, moving the original point $p_0(x_0, y_0)$ to an intermediate point $p_c(x_c, y_c)$. The next step is $r(\theta)$, moving the intermediate point $p_c(x_c, y_c)$ to the final point $p(x_1, y_1)$ by camera rotation around the Y axis. Therefore, the angles of ego-rotational motion of pan and tilt can be obtained as

$$\phi = \tan^{-1}\frac{y_c}{f} - \tan^{-1}\frac{y_0}{f}, \theta = \tan^{-1}\frac{x_c}{f} - \tan^{-1}\frac{x_1}{f}$$

where the coordinates of the intersection point can derived as

$$x_c = fx_0\left[\frac{\left(f^2 + x_1^2 + y_1^2\right)}{\left(f^2 + y_0^2\right)\left(f^2 + x_1^2\right) - \left(x_0 y_1\right)^2}\right]^{1/2}$$

$$y_c = fy_1\left[\frac{\left(f^2 + x_0^2 + y_0^2\right)}{\left(f^2 + y_0^2\right)\left(f^2 + x_1^2\right) - \left(x_0 y_1\right)^2}\right]^{1/2}$$

Notably, this is an ego-rotational motion model of one CCD when two successive images at two different times are captured.

IV. Ego-Rotational Motion Of Superposition Spherical Compound-like Eye

Based on images of an SSCE generated from CV, the rotational motion using an SSCE can be resolved using the following procedures.

1) Each camera in the SSCE whose image is ambiguous is the same as an ommatidium, and image fuzziness is independent. An ambiguous image can be achieved by adding random noises to an ideal image.
2) When the SSCE looks at an object, each ommatidium CCD perceives a different profile in the SSCE according to different locations of CCDs. In this manner, the compound-like eyes observe a entire ambiguous image, which is composed of many small, different, independent and ambiguous patterns.
3) When an object moves, the SSCE detects this rotation using two complete images, one before and one after the motion.
4) The process for generating the image for each CCD camera is the same as procedures 1–3.
5) Using those two vague images that include the rotational information, the corresponding intersection point for each camera can be estimated.
6) Any single CCD camera can generate a pair of pan and tilt angles with its intersection point. However, the number of cameras is positively correlated with the size of pan and tilt angles.
7) Taking the mean of all CCD camera ego-rotation angles, pan and tilt, unlike using standard least squares in ego-translation [23], ego-motion angles of pan and tilt of the SSCE can be obtained easily.

In this manner, when the amount of ommatidium CCD cameras is increasing, the ego-motion angles of an SSCE will increase. That the SSCE can obtain accurate ego-rotation angles even in the case of large noise is explored.

V. Experimental Results

To verify the performance of noise immunity for the SSCE, a given synthesized cloud of 50 3D points (Fig. 3) is chosen as the test object. To simulate a realistic situation, noise is introduced into ideal data. Assume image components in the ideal motion field (x, y) are perturbed by additive zero-mean Gaussian noise. The two noise processes in the x and y image planes were independent, and each was spatially uncorrelated. Variances of noise in error analysis conducted in [24]–[26] were given proportional to magnitudes of velocity components. To reflect actual implementation in computing optical flows using image patterns at adjacent time instants, the noise on the positions of image pixels and their variances was assumed constant over the entire image plane. Therefore, the image points contaminated by noise before and after a movement are modeled as

$$\begin{bmatrix} x_1(i)+N_{x1}(i) \\ y_1(i)+N_{y1}(i) \end{bmatrix} \text{ and } \begin{bmatrix} x_2(i)+N_{x2}(i) \\ y_2(i)+N_{y2}(i) \end{bmatrix},$$

where i indexes the image point, $(x(i), y(i))$ locates the ideal image point for the i-th point, and $N(i)$ is a zero-mean Gaussian random noise at this position. The noise processes N_{x1}, N_{y1}, N_{x2} and N_{y2} are assumed to have the same statistical property, and are given by

$$E\{N_{x1}^2(i)\} = E\{N_{y1}^2(i)\} = E\{N_{x2}^2(i)\} = E\{N_{y2}^2(i)\} = \sigma^2,$$

where σ is the standard deviation. In other words, all image points are contaminated by a random noise with the same variance.

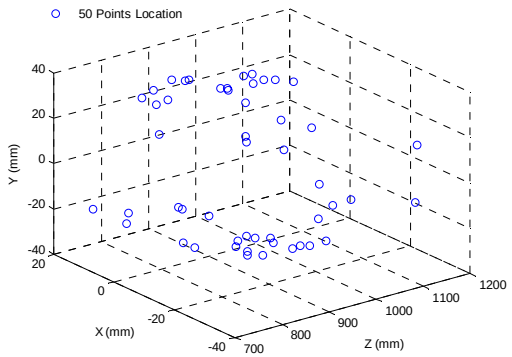

Fig. 3 A synthesized cloud of 50 3D points.

For the sake of simplification for the subsequent validation and simulation, we define relative error in the pan-tilt rotational angles as

$$err = \frac{\sqrt{(\phi^* - \phi)^2 + (\theta^* - \theta)^2}}{\sqrt{\phi^2 + \theta^2}}$$

where (ϕ^*, θ^*) is the computed pan-tilt ego-rotational angle, and $(\phi, \theta) \neq 0$ is the actual pan-tilt rotational angle. To achieve statistically reasonable results, 300 trials were conducted by increasing the number of CCD cameras for each situation. For rotational motions, the relative errors of the SSCE are, ideally, equal to zero.

For the purpose of validation, the SSCE is divided into two types: a non-fixed total length and width SSCE; and, fixed total length and width SSCE. The former is rotated on the X and Y axes at the same time using the same rotation angle interval, which extends to the left, right, upward, and downward with the same amount of CCD camera and non-fixed total rotation angle region, whereas, the latter is rotated on the X and Y axes simultaneously with same number of CCD cameras and using the fixed total region of the SSCE.

A. Non-Fixed Total Length and Width of the SSCE

The structural frame of the SSCE extends to four sides by a constant rotation angle interval of 10° for each CCD camera; that is, the total length and width of the complete SSCE varies based on the number of CCD cameras. Based on this arrangement, the rotational model of the SSCE can be formed (Fig. 1). This outcome is the complete SSCE, which is different from the single-row SSCE. Basically, the complete SSCE is generated that can set any rotation angle and the number of CCD cameras; however, the total number of CCD cameras must be even. Consequently, the number of SSCEs becomes $(2n+1)x(2n+1)$. However, for general applications, an odd number of CCD cameras can be utilized by shifting the center point of the SSCE.

This work selects only 1×1 to 9×9 SSCEs for the validation experiments and extend the variance of noise from 25–2500. Under different numbers of CCD cameras in the complete SSCE, when noise variance changes from small to large, the performance of different CCD cameras in the complete SSCE using the proposed algorithm can be compared. The 9×9 SSCE under the rotational motion of pan -9° and tilt 7° for the noise variance adding different noise levels at two time instants (red and black) (Fig. 4). The increasing noise variances make the image increasingly ambiguous, and the interference also increases. When noise variance is greater than 900, the noisy images (Figs. 4(d)–(f)) are all not easily distinguished from the original image. Even so, the proposed approach achieves very small relative errors for rotational motion (Table 1).

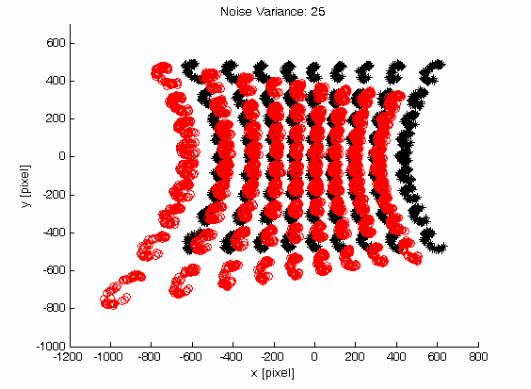

(a)

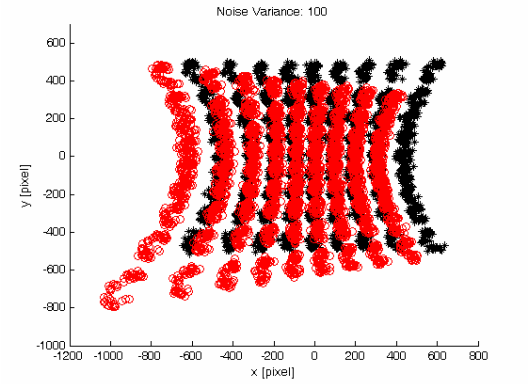

(b)

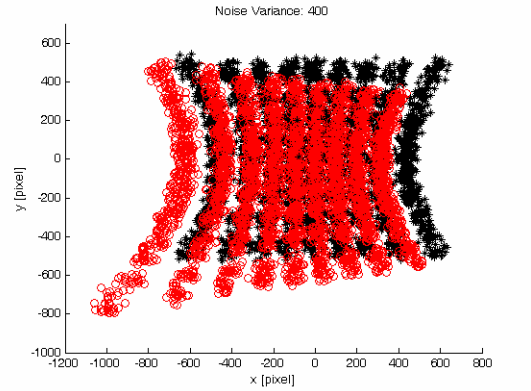

(c)

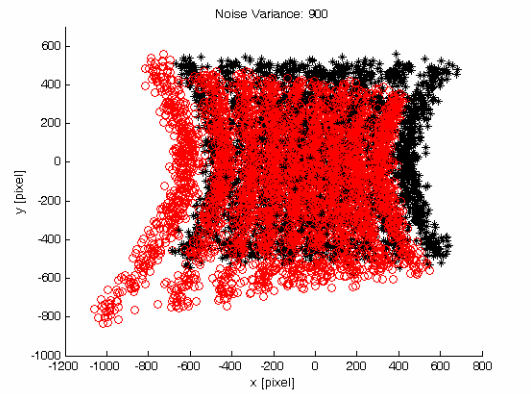

(d)

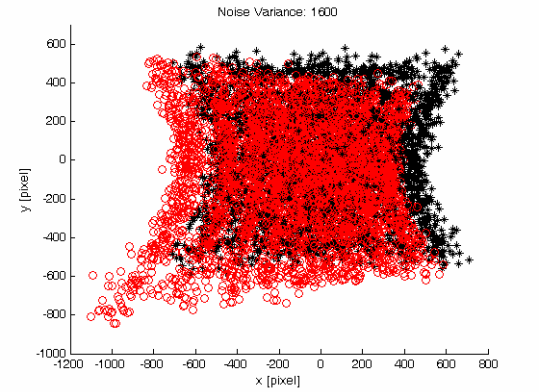

(e)

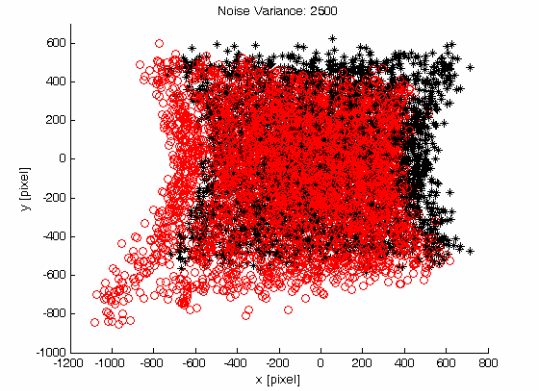

(f)

Fig. 4 The image points with different noise variances for the 9×9 complete SSCE at two time instants (red and black).

TABLE 1
RELATIVE ERRORS IN PERCENT OF THE EGO-ROTATION FOR DIFFERENT SSCE CONFIGURATIONS BY NON-FIXED TOTAL LENGTH AND WIDTH WITH VARIOUS NOISE VARIANCES

Variances	1x1	2x2	3x3	4x4	5x5	6x6	7x7	8x8	9x9
25	1.19	0.58	0.38	0.28	0.23	0.18	0.15	0.13	0.11
100	2.39	1.13	0.77	0.57	0.45	0.36	0.31	0.25	0.22
400	4.68	2.38	1.52	1.08	0.91	0.72	0.63	0.50	0.45
900	7.14	3.58	2.24	1.67	1.35	1.08	0.92	0.82	0.69
1600	9.45	4.56	3.09	2.47	1.89	1.43	1.23	1.02	0.88
2500	11.84	5.93	3.86	2.83	2.26	1.88	1.55	1.32	1.11

B. Fixed Total Length and Width of the SSCE

With fixed total length and width of the SSCE, this work validated the noise-resistance capability of a compound eye with an increased number of CCD cameras and a variable angle interval between cameras. When the total length and width of the complete SSCE is fixed, then the interval between CCD cameras will be a variable and change based on the number of CCD cameras. When the number of CCD cameras increases in the SSCE sphere, angle interval decreases, meaning that the density of the SSCE increases simultaneously. Assume each extended angle is 120° in the vertical and horizontal directions. The arrangements of SSCE were modified to 1x1, 3x3, 5x5, 7x7, 9x9, 11x11, 13x13, and 15x15. Following the preceding

manner of pan-tilt rotation, these different configurations are put into the extended angle area.

In this case, performance comparison was conducted by utilizing different numbers of cameras under different levels of additive noise, as described in Section A. Table 2 presents the results of the complete SSCE with fixed total length and width for different cases, and lists the relative errors for the SSCE arrangements under the effect of different noise levels.

TABLE 2
RELATIVE ERRORS IN PERCENT OF THE EGO-ROTATION FOR DIFFERENT SSCE CONFIGURATIONS BY FIXED TOTAL LENGTH AND WIDTH WITH VARIOUS NOISE VARIANCES UNDER LARGER ROTATION

Variances	1x1	3x3	5x5	7x7	9x9	11x11	13x13	15x15
25	1.14	0.33	0.19	0.13	0.11	0.09	0.08	0.07
100	2.19	0.64	0.38	0.27	0.23	0.18	0.16	0.14
400	4.61	1.27	0.76	0.55	0.42	0.38	0.30	0.26
900	7.09	1.91	1.29	0.83	0.65	0.53	0.49	0.44
1600	9.92	2.39	1.47	1.10	0.86	0.72	0.65	0.55
2500	11.47	3.10	2.02	1.39	1.05	0.88	0.77	0.67

When each extended angle reached 120° in the vertical and horizontal directions, and the rotational motion reduced to 7° and -5° in pan and tilt, respectively, the resulted relative errors are summarized in Table 3. The grace influence of immunity to noise in Tables 2 and 3 was also demonstrated.

TABLE 3
RELATIVE ERRORS IN PERCENT OF THE EGO-ROTATION FOR DIFFERENT SSCE CONFIGURATIONS BY FIXED TOTAL LENGTH AND WIDTH WITH VARIOUS NOISE VARIANCES UNDER SMALLER ROTATION

Variances	1x1	3x3	5x5	7x7	9x9	11x11	13x13	15x15
25	1.56	0.43	0.26	0.19	0.15	0.12	0.10	0.09
100	3.05	0.87	0.56	0.38	0.31	0.24	0.20	0.19
400	6.21	1.69	1.03	0.76	0.57	0.51	0.40	0.39
900	9.63	2.54	1.62	1.20	0.89	0.77	0.62	0.58
1600	12.74	3.27	2.09	1.50	1.20	0.99	0.82	0.76
2500	15.17	4.30	2.67	1.92	1.45	1.21	1.04	0.92

Weng et al. [27] proposed that the motion displacement should be large to allow stable estimation of motion and structure. In the above two cases, when the motion displacement is small, the sensitivity to noise is high, while the bearing capability of noise-resistance is low. When the motion displacement is increasing, the reliability of performance will get improved and the noise-resistance will increase. Next, comparing Tables 2 and 3 with the noise variance 2500, taking 15x15 for example, the relative errors for larger rotation (e.g., pan -9° and tilt 7°) and smaller rotation (e.g., pan 7° and tilt -5°) are 0.67 and 0.92, respectively. From the above discussion, this situation has been confirmed.

C. Discussion

Under these two different configurations—non-fixed and fixed total length and width of the complete SSCE—a number of conclusions are summarized

1) Regardless of whether total length and width of the SSCE are non-fixed or fixed, and rotation angle adopted, if the number of CCD cameras increases, noise resistance capability of the SSCE improves, even under the condition with high noise interference. For instance, with noise variance of 2500 (Tables 1 and 2), relative error decreased from 11.84% to 1.11% and from 11.47% to 0.67%, at 9x9 in Table1, 15x15 in Table 2, respectively depending on the arrangement of CCD cameras.
2) A dragonfly, which hunts during flight, has approximately 30000 ommatidia in each eye, whereas butterflies and moths, which do not hunt during flight, have only 12000–17000 ommatidia [12]. The obvious difference between these insects is the amount of ommatidia. Based on experimental results (Table 1), when the number of ommatidium in an insect increases, response to moving objects improves. In other words, as number of ommatidium an insect have increased, its ability to detect prey increases.
3) Numerous insects have a forward- or upward-pointing regions of high acuity, related either to the capture of prey, or to the pursuit of females by flying males. Although both sexes have specialized predation behaviors, it is only the male that has the acute zone indicative of its role in sexual pursuit. Acute zones vary considerably. In describing acute zones it is useful to indicate how densely an ommatidial array samples different regions in the surrounding environment [19]. Our experimental results exactly respond to this situation. When CCD camera density increases, the detection accuracy of compound-like eye improves (Tables 2 and 3). Consequently, the compound-like eye is able to provide a very accurate detection capability in 3D ego-motion.

VI. CONCLUSION

The compound eyes of flying insects are highly evolved organs. Although images received by their eyes are ambiguous, these insects are still capable of capturing prey so accurately and quickly. Inspired by these insects, pinhole image formation geometry has been applied to investigate the behavior of SSCEs when capturing moving objects. The concept underlying SSCE configuration and the ego-rotation model of SSCEs for pan-tilt motion are proposed.

Based on the number of ommatidia and acute zones in a compound eye, and through experiments in non-fixed and fixed total length and width SSCEs, this study determined that the total number and density of ommatidia are crucial factors to insect compound eyes. Those two influential factors very clearly correspond to experimental results obtained in this study. Notably, this work did not use any filters or optimization algorithm. Through these experiments, and based on the validation of the proposed algorithm, this work verified that insect compound eyes are powerful and excellent devices for detecting motion.

REFERENCES

[1] J. Tanida, T. Kumagai, K. Yamada, S. Miyatake, K. Ishida, T. Morimoto, N. Kondou, D. Miyazaki, and Y. Ichioka, "Thin observation module by bound optics (TOMBO): concept and experimental verification," *Applied Optics*, Vol. 40, No. 11, pp. 1806-1813, 2001.

[2] R. Ng, Marc Levoy, M. Bredif, G. Duval, M. Horowitz, and P. Hanrahan, "Light field photography with a hand-held plenoptic camera," Stanford University Computer Science, Tech Report CSTR 2005-02, 2005.

[3] E. H. Adelson and J. Y. A. Wang, "Single lens stereo with a plenoptic camera," *IEEE Trans. PAMI*, vol. 14, pp. 99-106, 1992.

[4] T. Netter and N. Franceschini, "A robotic aircraft that follows terrain using a neuro-morphic eye," in *IEEE Proceedings of Conference on Intelligent Robots and Systems*, pp. 129-134, 2002.

[5] K. Hoshino, F. Mura, H. Morii, K. Suematsu, and I. Shimoyama, "A small-sized panoramic scanning visual sensor inspired by the fly's compound eye," in *IEEE Proceedings of Conference on Robotics and Automation*, pp. 1641-1646, 1998.

[6] R. Volkel, M. Eisner, and K.J. Weible, "Miniaturized imaging system," *J. Microelectronic Engineering*, Elsevier Science, 67-68, pp. 461-472, 2003.

[7] R. Hornsey, P. Thomas, W. Wong, S. Pepic, K. Yip and R. Krishnasamy, "Electronic compound eye image sensor: construction and calibration," in *Sensors and Camera Systems for Scientific, Industrial, and Digital Photography Applications V*, M.MBlouke, N.Sampat, R.Motta, eds., Proc. SPIE 5301, pp. 13-24, 2004.

[8] J. Neumann, C. Fermuller, Y. Aloimonos, and V. Brajovic, "Compound eye sensor for 3D ego motion estimation," in *IEEE Proceedings of Conference on Intelligent Robots and Systems* , Vol. 4, pp. 3712-3717, 2004.

[9] J. Kim, K.H. Jeong and L.P. Lee, "Artificial ommatidia by self-aligned microlenses and waveguides," *Opt. Express*, 30, pp. 5-7, 2005.

[10] C.L. Tisse, "Low-cost miniature wide-angle imaging for self-motion estimation," *Optics Express*, Vol. 13, No. 16, pp. 6061-6072, 2005.

[11] John W. Kimball, "The compound eye," Kimball's Biology Pages, http://users.rcn.com/jkimball.ma.ultranet/BiologyPages/C/CompoundEye.html

[12] M. Elwell and L. Wen, "The power of compound eyes," *Optics & Photonics News*, pp. 58-59, 1991.

[13] G.A. Horridge, "A theory of insect vision: velocity parallax," *Proc. of the Royal Society of London B*, vol. 229, pp.13-27, 1986.

[14] E.C. Sobel, "The locust's use of motion parallax to estimate distance," *J. Comp. Physiol. A*, vol. 167, pp. 579-588, 1990.

[15] M. V. Srinivasan, S. W. Zhang, M. Lehrer, T. S. Collett, "Honeybee navigation EN ROUTE to the goal: visual flight control and odometry," *The Journal of Experimental Biology*, vol. 199, pp. 237-244, 1996.

[16] T. Collett, "Animal behaviour: Survey flights in honeybees," *Nature*, vol. 403, pp. 488-489, Feb 2000.

[17] G. L. Lin and C. C. Cheng, "Single-row superposition-type spherical compound-like eye for pan-tilt motion recovery," in *2007 IEEE SSCI: 2007 IEEE Symposium on Computational Intelligence in Image and Signal Processing*, pp. 24-29, 2007.

[18] W. S. Romoser, *The Science of Entomology*, Macmillian Publishing Co., Inc., 1973.

[19] M. F. Land and D-E Nilsson, *Animal Eyes*, Oxford University Press, 2002.

[20] Y. Aloimonos, New Camera Technology: Eyes from Eyes. Available: http://www.cfar.umd.edu/~larson/dialogue/newCameraTech.html

[21] K. Prazdny, "Determining the instantaneous direction of motion from optical flow generated by a curvilinear moving observer," *Computer Graphics Image Processing*, vol. 17, pp. 238-248, 1981.

[22] W. Burger and B. Bhanu, "Estimating 3-D egomotion from perspective image sequences," *IEEE Trans. PAMI*, vol. 12, pp. 1040-1058, 1990.

[23] G. L. Lin and C. C. Cheng, "Single-Row superposition-type compound-like eye for motion recovery," in *IEEE International Conference on Systems, Man and Cybernetics*, pp. 1986-1991, 2006.

[24] E. Simoncelli, E. Adelson, and D. Heeger, "Probability distributions of optical flow," in *Proc. IEEE Int. Conf. Computer Vision and Pattern Recognition*, Mauii, Hawaii, 1991, pp. 310–315.

[25] J. L. Barron, D. J. Fleet, and S. S. Beauchemin, "Performance of optical flow techniques," *International Journal of Computer Vision*, vol. 13, no. 1, pp. 43–77, Sep. 1994.

[26] N. Gupta and L. Kanal, "3-D motion estimation from motion field," *Artificial Intelligence*, vol. 78, pp. 45–86, Nov. 1995.

[27] J. Weng, T. S. Huang and N. Ahuja, "Motion and structure from two perspective views: algorithms, error analysis, and error estimation", *IEEE Trans. PAMI*, vol. 11, pp. 451-476, 1989.